

Probing the Cl–HCl complex via bond-specific photodissociation of (HCl)₂

K. Liu, A. Kolessov, J.W. Partin, I. Bezel, C. Wittig *

Department of Chemistry, University of Southern California, Los Angeles, CA 90089, USA

Received 7 October 1998; in final form 26 October 1998

Abstract

Infrared–ultraviolet double resonance has been used to photodissociate the free HCl bond of the HCl dimer. This creates Cl–HCl in a coherent superposition of electronic and vibrational states. Measurement of the translational energy of the departing H atom using high-*n* Rydberg time-of-flight spectroscopy enables the Cl–HCl potential surfaces to be probed. The features thus obtained agree with theoretical estimates. At long IR–UV delays, the fastest H atoms derive primarily from UV photodissociation of internally excited HCl (e.g., high rotational levels) formed by (HCl)₂ predissociation. © 1999 Elsevier Science B.V. All rights reserved.

1. Introduction

Photoinitiated processes in weakly-bound clusters provide opportunities to elucidate a number of interactions and mechanisms in chemical reaction dynamics [1–7]. Of these, long-range inter-molecular forces that influence chemical reactions by orienting reactive species have been of particular interest [8–10]. To this end, weakly-bound complexes of halogen atoms and hydrogen halide molecules (i.e., X–HY) have emerged as important prototypes for examining entrance valley properties of reactive X + HY → HX + Y potential energy surfaces (PESs). In the case of Cl–HCl, Dubernet and Hutson have calculated long-range features of the non-reactive portions of the atom–molecule PESs, including anisotropy and atomic spin–orbit coupling [10]. Interactions between HCl and the Cl-atom ²P_{1/2} and ²P_{3/2} states

result in three weakly-bound, adiabatic PESs; the lower two correlate to ²P_{3/2}, while the upper one correlates to ²P_{1/2}. The two ²P_{3/2} adiabats derive from different projections of the total (orbital plus spin) electronic angular momentum along the inter-molecular axis. Experimental characterization of these potentials would provide a test of our understanding of the long-range interactions present in elementary hydrogen exchange reactions.

In a study of the 266 nm photodissociation of the L-shaped HI dimer using high-*n* Rydberg time-of-flight (HRTOF) spectroscopy, Zhang et al. have noted that photolytic removal of the free (i.e., non-hydrogen-bonded) hydrogen from (HI)₂ yields fragments whose properties can be described in analogy to those of the Cl–HCl system [2]. It was pointed out that such a photoinitiated process launches a wavepacket on the atom–molecule adiabats, thereby sampling the long-range part of the exchange reaction PESs. However, the inability to select (i) the

* Corresponding author. E-mail: wittig@chem1.usc.edu

cluster size and (ii) the specific HI moiety being photodissociated precluded the possibility of a complete assignment of the observed translational energy distributions.

For the $(\text{HCl})_2$ system, Gerber and co-workers have investigated its photodissociation dynamics at 193 nm by using classical trajectory simulations, in which the Cl–HCl interaction was approximated by the closed-shell atom–molecule potential of Ar–HCl [11]. Moreover, it has been suggested [11,12] and demonstrated [13] that bond- and/or state-specific and size-selective photolysis of clusters can be achieved by using multiple-resonance techniques.

In this Letter, preliminary results are reported of an IR + UV double resonance (DR) photodissociation study of the HCl dimer ‘tagged’ by vibrationally exciting the first overtone of the HCl moiety which serves as a hydrogen-bond acceptor. This has allowed us to identify bond-specific photochemical and vibrational predissociation dynamics from the dimer. In particular, H-atom time-of-flight features have been observed which are associated with the direct photodissociation of the tagged dimers.

The method employed here complements that described by Nesbitt and co-workers for probing quan-

tum state-selected photodissociation dynamics of Ar-H_2 [13,14]. In our approach, the distribution of internal excitation of the photofragment Cl–HCl is encoded in the translational energy distribution of the recoiling H, which is recorded by using the HRTOF technique [15,16]. The first overtone transitions used for tagging the dimer are measured by using IR cavity ringdown laser absorption spectroscopy (CRLAS), as reported previously [17].

2. Experimental

The experimental strategy is illustrated in Fig. 1. HCl dimer is selectively excited near $1.77 \mu\text{m}$ to the first overtone ($2\nu_1$) vibration–rotation–tunneling (VRT) levels of the free HCl bond. Subsequently, 193.3 nm radiation dissociates preferentially the vibrationally excited hydrogen-bond acceptor due to the increased Franck–Condon overlap brought about by vibrational excitation of the acceptor HCl moiety. The absorption cross-section for the unexcited donor HCl moiety remains relatively low. Excited dimers may also undergo vibrational predissociation, resulting in correlated product state distributions of the

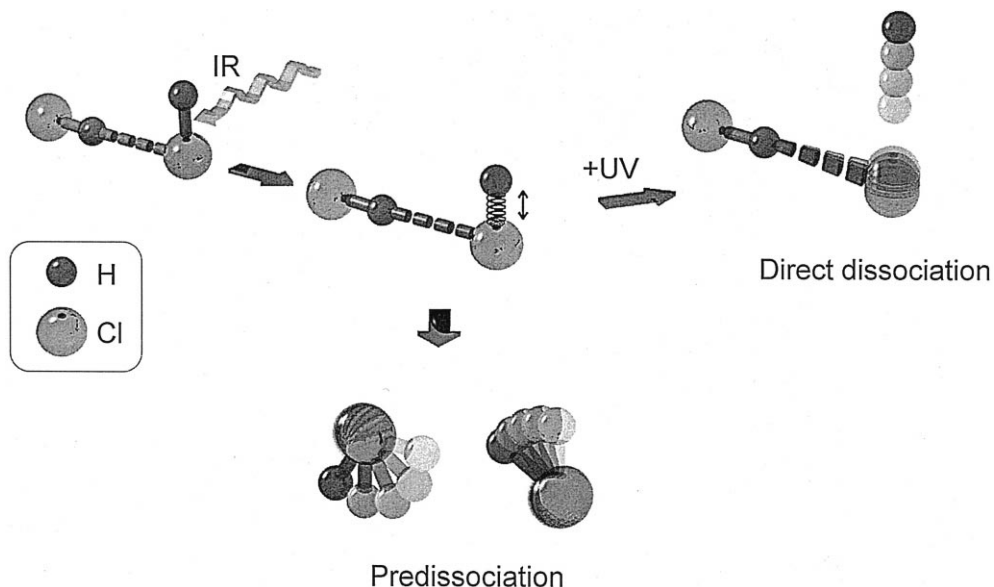


Fig. 1. An IR photon excites the free HCl bond, thereby ‘tagging’ the cluster. The lower pathway shows predissociation; the donor HCl is expected to acquire much more angular momentum than the acceptor. The other pathway is UV photodissociation of the tagged dimer; the H atom leaves behind the Cl–HCl complex.

monomer pairs. This is expected to occur with low (acceptor) and high (donor) rotational excitation – as has been observed in the case of $(\text{HF})_2$ [18,19]. The vibrational predissociation lifetime of the $2\nu_1$ level of the dimer is estimated to be ≥ 3 ns, based on the linewidth measured by using CRLAS [17]. Both the tagged dimer and internally excited monomers produced via predissociation can be photolyzed by the UV to produce H-atom TOF spectra. By varying the delay between the IR and UV lasers, it is possible to separate the contributions from these two sources of fast H atoms.

The HRTOF apparatus has been described previously [20]. A cavity ringdown spectrometer has been integrated into the setup to locate the VRT transitions of the dimer [17]. Fig. 2 shows the combined CRLAS–DR–HRTOF arrangement. Jet-cooled HCl dimers were generated in a pulsed supersonic expansion of a mixture of 7% HCl in Ar at a stagnation pressure of 2.3 atm through a 1.2 mm dia. pulsed nozzle. The position of the nozzle was adjusted between the ringdown and DR experiments. Tunable IR radiation (linewidth ~ 0.015 cm^{-1}) was produced in an OPO (STI Mirage 3000) capable of

long-term locking to a single mode (Laser Vision). Typically, 15–25 mJ at 1.77 μm was focused with a 50 cm *f.l.* quartz lens into the photolysis chamber. Before focusing, the beam was deflected by a mirror installed on a rotary kinematic mount for carrying out the CRLAS measurements. Photodissociation was done with an ArF excimer laser (unstable resonator, 4–12 mJ, jitter ≤ 5 ns) counter-propagating to the IR beam. Two other counter-propagating beams (121.6 and 366 nm) excited H atoms to high- n Rydberg states. The translational energy distribution of the tagged H atoms was obtained from the TOF distributions. For the DR experiments, data were collected with the IR laser alternately on and off.

For the DR studies, the IR laser was tuned to the Q branch transitions of the $\Delta K_a = 1 \leftarrow 0$, $2\nu_1^+$ VRT subband of $(\text{H}^{35}\text{Cl})_2$, where the (+) sign represents transitions originating from the lower exchange tunneling level of the dimer ground state [17]. Because of the overlapping $Q(J)$ lines, several VRT transitions could be pumped simultaneously; this is not expected to significantly affect the dynamics discussed below. For calibration purposes, the IR laser has also been scanned to the first overtone $\text{R}(0)$

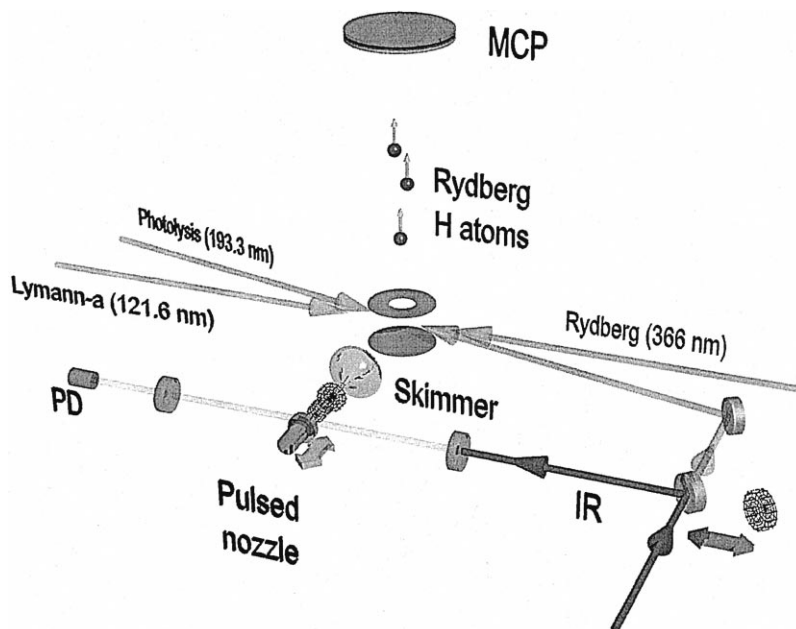


Fig. 2. Experimental arrangement in which CRLAS and HRTOF are combined (PD = photodiode; MCP = microchannel plate). Wired versions of the nozzle and mirror indicate their positions in the HRTOF experiment.

transition of the H^{35}Cl monomer and its DR TOF spectrum has been recorded.

3. Results and discussion

Fig. 3 shows translational energy distributions obtained from the HRTOF distributions; (a) and (b) correspond to the UV photolysis pulse delayed 10

and 70 ns, respectively, relative to the IR pulse. The pronounced doublets (left-hand sides) are due to Cl-atom $^2\text{P}_{3/2}$ and $^2\text{P}_{1/2}$ levels deriving from the photodissociation of HCl monomer. The broad features at the bases of the doublets are believed to be due to clusters, with the respective contributions from different cluster sizes unknown. Similar results have been obtained with Ar–HBr [1] and $(\text{HI})_2$ [2].

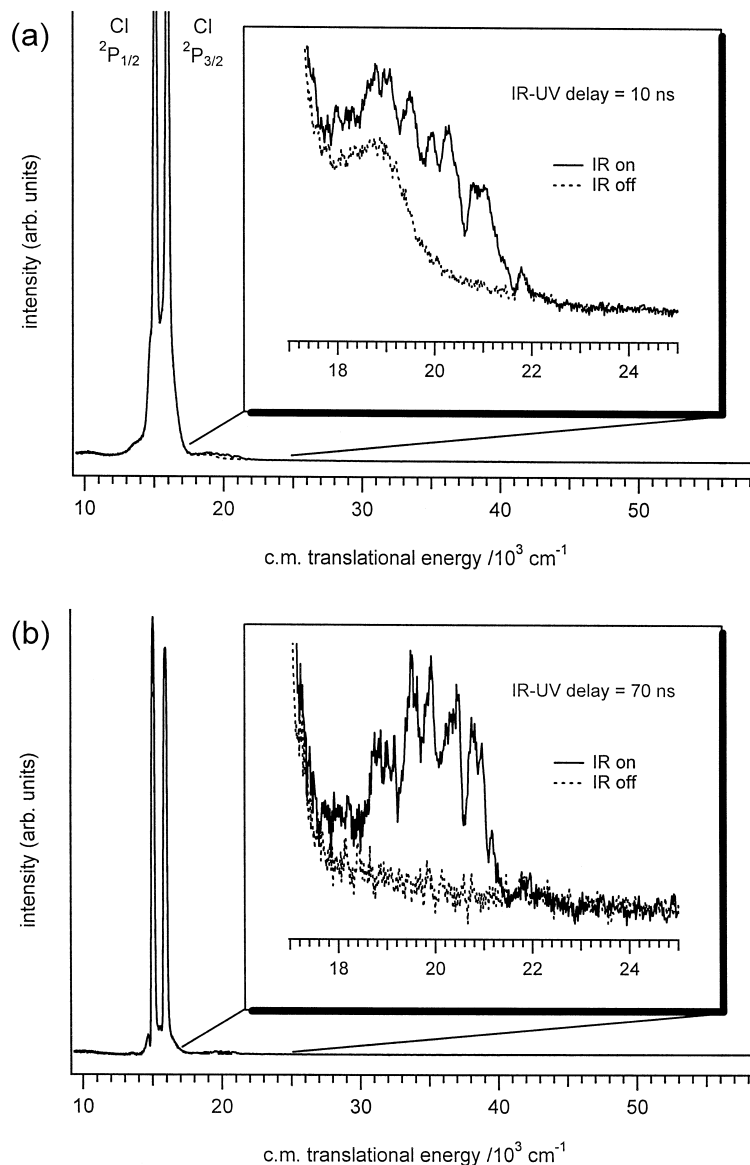


Fig. 3. Center-of-mass translational energy distributions; the UV pulse is delayed relative to the IR pulse: (a) 10 ns and (b) 70 ns. Solid and broken lines indicate IR on and off, respectively.

The effect of IR excitation of the HCl dimer is shown in the magnified insets of Fig. 3. Signal averaging is responsible for the different signal-to-noise ratios (S/N_s) in (a) and (b). The signal at 70 ns delay derives mainly from predissociated monomer pairs, while the short delay data contain contributions from both direct and predissociation channels. We do not know the predissociation lifetime (τ_{PD}) of the dimer at the first overtone of the free HCl. However, on the basis of studies of the vibrational dependence of the predissociation lifetime in $(HF)_2$ [21–23] and the predissociation of $(HCl)_2$ at the free fundamental ($\tau_{PD} \geq 100$ ns), we assume that the lifetime of $(HCl)_2$ in the $2\nu_1$ level does not exceed 100 ns. This is consistent with the fact that similar structure has been observed at delays up to 500 ns. The peaks in the DR signal (i.e., the difference spectrum between IR on and off) lie at energies which correspond to highly excited HCl. For example, the two highest-energy peaks in the 70 ns distribution differ by the energy difference between $J = 20$ and 21 of $HCl(v = 0)$. High rotational excitation of the donor has been noted previously for the HF system [19]. In the present case, it is amusing that two quanta of vibrational energy in the free HCl are transferred to internal excitation of one of the recoiling monomers (presumably the donor) upon predissociation. This came as a surprise.

The photochemical process of most interest is $(HCl)_2^+ + h\nu_{UV} \rightarrow H + Cl-HCl$. Signals from this channel can be obtained from differences between DR spectra taken at short and long delays (see Fig. 4). Indeed, such a contribution is identified in the difference spectrum shown in Fig. 4b. For comparison, Fig. 4c displays the DR spectrum of $H^{35}Cl$ monomer tagged by the first overtone $R(0)$ transition.

Because of the large H vs. Cl mass difference, H-atom departure occurs with little concomitant change of the Cl–Cl distance. To a first approximation the intact HCl acts as a spectator to the dissociation event. Thus the departing H atom receives 35/36 of the available translational energy in the c.m. system of the dissociating HCl moiety, and the Cl atom receives 1/36 (i.e., ~ 600 cm^{-1}). Of this 600 cm^{-1} , approximately half is partitioned into vibrational and rotational energy of Cl–HCl in the $(HCl)_2$ c.m. system. The other half goes into translational

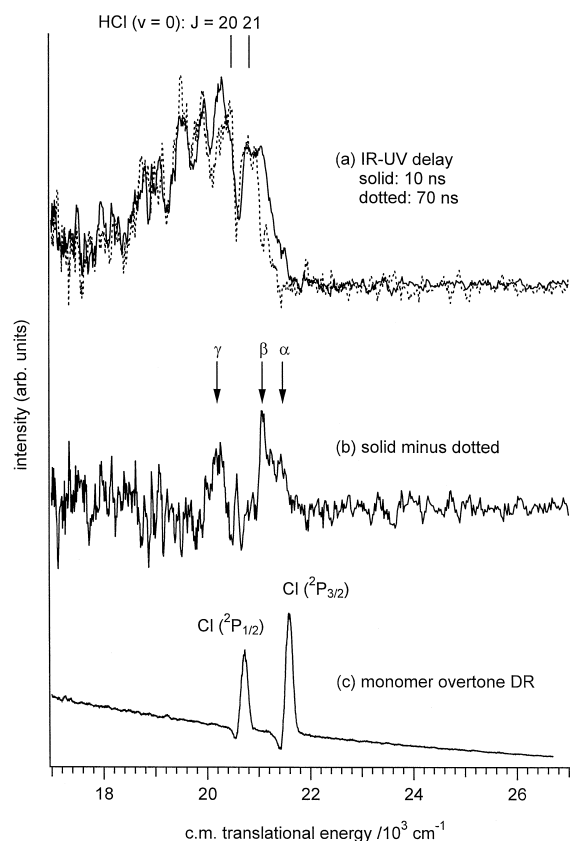


Fig. 4. Photodissociation of tagged dimers is identified by subtracting the 70 and 10 ns traces; (a) shows the traces and (b) shows the difference; (c) shows $Cl(^2P_{3/2})$ and $Cl(^2P_{1/2})$ deriving from photodissociation of overtone-excited HCl monomer.

energy of the Cl–HCl complex relative to the $(HCl)_2$ c.m. This follows from the fact that Cl–HCl is approximately twice as heavy as Cl, and therefore from momentum conservation the speed of Cl–HCl relative to the $(HCl)_2$ c.m. system is approximately half that of Cl relative to the HCl c.m. system.

The departing H atom carries information about the Cl–HCl complex left behind. This complex does not undergo significant decomposition on the rapid timescale characteristic of H-atom removal. At low resolution, one can expect to see the Cl atom $^2P_{3/2}$ and $^2P_{1/2}$ levels, whereas with better resolution, the PESs of the Cl–HCl system will be reflected. Note that rapid H-atom removal creates a coherent superposition of electronic and vibrational levels of the Cl–HCl complex. At even higher resolution (not yet available), it may be possible to resolve vibrational

structure and widths arising from Cl–HCl decomposition.

The trace shown in Fig. 4b, despite its low S/N, reflects the PESs of Cl–HCl. Though the two main features are undoubtedly associated with the Cl spin–orbit levels, they are broader than those associated with unclustered Cl (Fig. 4c). We believe that this broadening is real and due to Cl–HCl vibrational and electronic excitations; it is present at all levels of signal averaging.

Fig. 5 shows some relevant energies. For HCl monomer, energy balance is given by:

$$KE^{\text{mon}} = h\nu_{193} + h\nu_{R(0)} - D_{0,j}^{\text{mon}}, \quad (1)$$

where KE^{mon} is the c.m. translational energy of HCl monomer. The dissociation energy, $D_{0,j}^{\text{mon}}$, is 35750 cm^{-1} for $j = 3/2$ [i.e., $\text{Cl}(^2\text{P}_{3/2})$] and 36630 for $j = 1/2$ [i.e., $\text{Cl}(^2\text{P}_{1/2})$]. Eq. (1) yields KE^{mon} values of 21670 and 20790 cm^{-1} for $^2\text{P}_{3/2}$ and $^2\text{P}_{1/2}$, respectively. These values are close to the peak positions shown in Fig. 4c. For HCl dimer, an approximate upper bound is given by:

$$KE_{\text{max}}^{\text{dimer}} = h\nu_{193} + h\nu_{Q(j)} - \Delta E_{\text{zp}} - D_{0,3/2}^{\text{mon}}, \quad (2)$$

where ΔE_{zp} is the difference between the zero-point

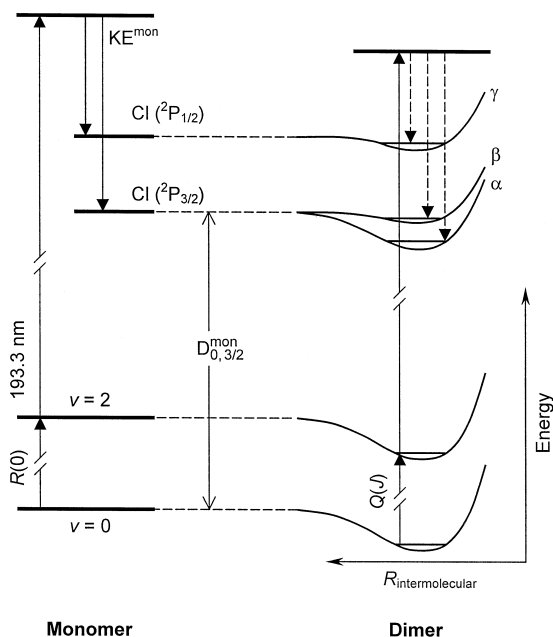


Fig. 5. Energy diagram for direct photodissociation processes in HCl monomer and dimer.

binding energies of $(\text{HCl})_2$ and the lowest adiabat of Cl–HCl. By using an $(\text{HCl})_2$ binding energy of $431 \pm 22 \text{ cm}^{-1}$ [24] and a well depth of 380 cm^{-1} relative to $\text{Cl}(^2\text{P}_{3/2}) + \text{HCl}$ for the lowest Cl–HCl adiabat [10], Eq. (2) predicts that $KE_{\text{max}}^{\text{dimer}}$ lies 90 cm^{-1} lower in energy than the $^2\text{P}_{3/2}$ monomer feature shown in Fig. 4c. This upper bound is labeled α in Fig. 4b. Likewise, using the well depth values for the other two adiabats calculated by Dubernet and Hutson [10] (i.e., 90 cm^{-1} relative to $\text{Cl}(^2\text{P}_{3/2}) + \text{HCl}$ and 130 cm^{-1} relative to $\text{Cl}(^2\text{P}_{1/2}) + \text{HCl}$), the upper bounds labeled β and γ in Fig. 4b are obtained. Namely, β is 380 cm^{-1} lower than the $^2\text{P}_{3/2}$ monomer feature and γ is 330 cm^{-1} lower than the $^2\text{P}_{1/2}$ monomer feature. The α , β , and γ values indicated in Fig. 4b are in accord with the experimental data. The above upper bounds do not include Cl–HCl zero-point energies, which are expected to be a few tens of wavenumbers – insignificant at the present resolution.

The translational energies in Figs. 3 and 4 assume that the relevant c.m. system is that of the HCl unit which undergoes photodissociation. This is unambiguous for HCl monomer. For HCl dimer, momentum balance is between H and Cl–HCl, even if the latter decomposes. However, the large H vs. Cl mass difference, as well as the weakly-bound nature of the dimer, enables momentum balance to be carried out (approximately) in the c.m. system of the dissociating HCl. Thus, a single transformation can be used for all of the data.

Resolution is currently limited by the excimer laser linewidth ($\sim 160 \text{ cm}^{-1}$), as revealed by the monomer widths. However, the dimer features are much broader than 160 cm^{-1} . This is believed to reflect mainly the fact that the free HCl bond dissociates with a range of recoil angles relative to the intermolecular axis with probabilities as per the squares of the acceptor bending wavefunction of the parent cluster, producing Cl–HCl complexes with a range of internal excitations. With improved resolution and S/N, one might observe vibrational structure, thereby providing a stringent test of the PESs.

4. Concluding remarks

The selection of cluster size and chemical bond has been achieved by using IR + UV double reso-

nance. This has enabled photodissociation dynamics of tagged HCl dimers to be studied. Specifically, H-atom removal from the free HCl moiety (thus forming the Cl–HCl complex) has been identified by using HRTOF spectroscopy, which uses the H atom as a probe of the internal energy distribution of the Cl–HCl photofragment. The translational energy distribution in this channel agrees with calculated PESs. As with the use of negative-ion photodetachment spectroscopy to probe transition state regions of XHY systems [7], the DR–HRTOF method is a promising tool for examining long-range interactions in chemically interesting systems.

Acknowledgements

This research was supported by the U.S. Department of Energy. The authors thank H. Reisler for valuable discussions and A. Bragg and A. Zivkovic for technical assistance.

References

- [1] J. Segall, Y. Wen, R. Singer, C. Wittig, A. Garcia-Vela, R.B. Gerber, *Chem. Phys. Lett.* 207 (1993) 504.
- [2] J. Zhang, M. Dulligan, J. Segall, Y. Wen, C. Wittig, *J. Phys. Chem.* 99 (1995) 13680.
- [3] Y. Chen, G. Hoffmann, S.K. Shin, D. Oh, S. Sharpe, Y.P. Zeng, R.A. Beaudet, C. Wittig, in: *Advances in Molecular Vibrations and Collision Dynamics*, vol. 1, Part B, JAI Press, Greenwich, CT, 1992, p. 187.
- [4] W.H. Breckenridge, C. Jouvet, B. Soep, *J. Chem. Phys.* 84 (1986) 1443.
- [5] B. Soep, S. Abbès, A. Keller, J.P. Visticot, *J. Chem. Phys.* 96 (1992) 440.
- [6] X.Y. Chang, R. Ehlich, A.J. Hudson, J.C. Polanyi, J.-X. Wang, *J. Chem. Phys.* 106 (1997) 3988.
- [7] D.M. Neumark, *Acc. Chem. Res.* 26 (1993) 33.
- [8] R.B. Metz, A. Weaver, S.E. Bradforth, T.N. Kitsopoulos, D.M. Neumark, *J. Phys. Chem.* 94 (1990) 1377.
- [9] V. Aquilanti, D. Cappelletti, F. Pirani, L.Y. Rusin, M.B. Sevryuk, J.P. Toennies, *J. Phys. Chem.* 95 (1991) 8248.
- [10] M.-L. Dubernet, J.M. Hutson, *J. Phys. Chem.* 98 (1994) 5844.
- [11] A.B. McCoy, Y. Hurwitz, R.B. Gerber, *J. Chem. Phys.* 97 (1993) 12516.
- [12] S.K. Shin, Y. Chen, E. Böhmer, C. Wittig, in: *Topics in Applied Physics*, vol. 70, Springer, Berlin, 1992, pp. 57–76.
- [13] D.F. Plusquellic, O. Votava, D.J. Nesbitt, *J. Chem. Phys.* 101 (1994) 6356.
- [14] O. Votava, J.R. Fair, D.F. Plusquellic, E. Riedle, D.J. Nesbitt, *J. Chem. Phys.* 107 (1997) 8854.
- [15] L. Schneider, W. Meier, K.H. Welge, M.N.R. Ashfold, C. Western, *J. Chem. Phys.* 92 (1990) 7027.
- [16] M.N.R. Ashfold, I.R. Lambert, D.H. Mordaunt, G.P. Morley, C.M. Western, *J. Phys. Chem.* 96 (1992) 2938.
- [17] K. Liu, M. Dulligan, I. Bezel, A. Kolessov, C. Wittig, *J. Chem. Phys.* 108 (1998) 9614.
- [18] L. Oudejans, R.E. Miller, W.L. Hase, *Faraday Discuss.* 102 (1995) 323.
- [19] L. Oudejans, R.E. Miller, *J. Phys. Chem. A* 101 (1997) 7582.
- [20] J. Zhang, C.W. Riehn, M. Dulligan, C. Wittig, *J. Chem. Phys.* 104 (1996) 7027.
- [21] A.S. Pine, W.J. Lafferty, B.J. Howard, *J. Chem. Phys.* 81 (1984) 2939.
- [22] A.S. Pine, G.T. Fraser, *J. Chem. Phys.* 89 (1988) 6636.
- [23] M.A. Suhm, J.T. Farrell Jr., A. McIlroy, D.J. Nesbitt, *J. Chem. Phys.* 97 (1992) 5341.
- [24] A.S. Pine, B.J. Howard, *J. Chem. Phys.* 84 (1986) 590.